Heliyon

Received:
8 September 2018
Revised:
6 December 2018
Accepted:
2 January 2019

Cite as: Monika Saini, Reetu Sangwan, Mohammad Faheem Khan, Ashok Kumar, Ruchi Verma, Sudha Jain. Specioside (SS) & verminoside (VS) (Iridoid glycosides): isolation, characterization and comparable quantum chemical studies using density functional theory (DFT). Heliyon 5 (2019) e01118. doi: 10.1016/j.heliyon.2019.e01118

Specioside (SS) & verminoside (VS) (Iridoid glycosides): isolation, characterization and comparable quantum chemical studies using density functional theory (DFT)

Monika Saini [a], **Reetu Sangwan** [a], **Mohammad Faheem Khan** [b], **Ashok Kumar** [a], **Ruchi Verma** [a], **Sudha Jain** [a,*]

[a] *Department of Chemistry, University of Lucknow, Lucknow, 226007, Uttar Pradesh, India*

[b] *Department of Biotechnology, Era Medical College, Era University, Lucknow, 226003, Uttar Pradesh, India*

[*] Corresponding author.

E-mail address: jainsudha2@rediffmail.com (S. Jain).

Abstract

Two biologically important molecules specioside (SS) and verminoside (VS) have been isolated from the ethanolic extract of stem bark of *Kigelia pinnata*. We have explored the electronic and spectroscopic properties of these two molecules on the basis of the Density Function Theory (DFT) quantum chemical calculations along with the correlations of biological efficacies and the results are presented in this paper. The structures of the molecules were established with the help of spectroscopic techniques (^{1}H, ^{13}C NMR, UV-VIS, FTIR) and chemical reactivity was compared by computed DFT theory using Becke3-Lee-Yang-Parr (B3LYP)/6-31G (d,p) data basis set. UV-Visible spectrum was obtained using Time Dependent DFT method. Electric dipole moment, polarizability, first static hyper polarizability and hyper conjugative interactions were also studied with the aid of natural bond orbital (NBO) analysis of these two compounds. The thermodynamic parameters of these compounds were determined at various

https://doi.org/10.1016/j.heliyon.2019.e01118

temperatures. The HOMO, LUMO, chemical hardness (η), chemical potential (μ), electronegativity (χ), electrophilicity power (ω), the gap energy and NBO analysis of both the compounds have been discussed in this paper. Local reactivity was evaluated through the Fukui function i.

Keywords: Natural product chemistry, Theoretical chemistry, Organic chemistry

1. Introduction

Kigelia pinata (Syn. *K. africana* and *K. aethiopia*) (Family Bignoniaceae), is an African tree widely grown in tropics and including India. The tree is commonly known as "sausage tree" because of the huge fruits hanging from the long fibrous stalks [1]. The rural community uses mostly all parts of the tree viz. fruit, bark, roots and leaves for various ailments [2, 3, 4]. The plant is reported to possess a wide spectrum of biological activities viz. analgesic, anti-inflammatory, antineoplastic, wound healing, antidiabetic, antioxidant, antiurolithic, anticonvulsant, antihypolipidimic and anti-amoebic activity [5]. Three iridoside monoterpenoids namely specioside (SS), verminoside (VS) and minecoside isolated from different parts of this plant [6, 7]. *K. pinanta* plant has shown *in vitro* antiamoebic activity against HK -9 strain of *Entamoeba histolytica*. The anti-amoebic activity of these compounds specioside (SS), verminoside (VS) and minecoside were isolated by the extract of the stem bark of *K. pinnata* plant. Verminoside (VS) has two fold antiamoebic activities as compared to the standard drug metronidazole while specioside (SS) showed comparable activity with the standard drug [8]. Other than this, specioside (SS) has been found to possess analgesic, antidyspeptic, astringent, liver stimulating and wound healing properties [9]. On contrast, verminoside (VS) showed anti-inflammatory, anti-microbial and anti-skin aging properties [10]. The polar extract of the fruit part of *K. pinnata* was significant the anti-inflammatory effects of verminoside (VS) that inhibiting both iNOS expression and NO release in the LPS-induced J774.A1 macrophage cell line [11]. The anti-ulcer activity of the ethanol extract of *Kigelia* plant stem bark in Wistar albino rats. In both preventive and curative models of ulcer respectively induced by absolute ethanol and indometacin, the extract caused marked inhibition of ulceration, suggesting a dose-dependent gastro-protective effect by the plant in the two models of ulcer [9]. The use of *Kigelia africana* to prevent or to treat cancer of the seed oil on cell proliferation in culture, human colon adenocarcinoma (Caco-2) and human embryonic kidney (HEK-293) cells were maintained and treated with various concentrations (0, 20, 40, 80, 100 and 120 mg/l) of *Kigelia africana* seed oil [12, 13]. A number of reports are available dealing with the quantum chemical studies, DFT and QTAIM approach to correlate the structure with biological properties of natural products [14, 15]. The chemical structure of both specioside (SS) and verminoside (VS) is nearly the same except

https://doi.org/10.1016/j.heliyon.2019.e01118

that verminoside (VS) has one extra hydroxy functional group which may be responsible for the different biological activities. Therefore, to correlate the chemical structure and biological activity we have compared structure activity of both the compounds on the basis of quantum chemical approach. The chemical structure and optimized structures of specioside (SS) and verminoside (VS) are shown in Figs. 1 and 2 respectively.

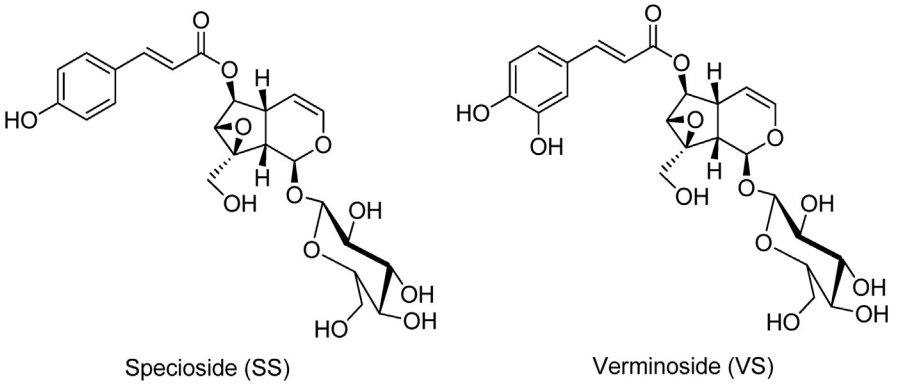

Fig. 1. Chemical structures of Specioside (SS) and Verminoside (VS).

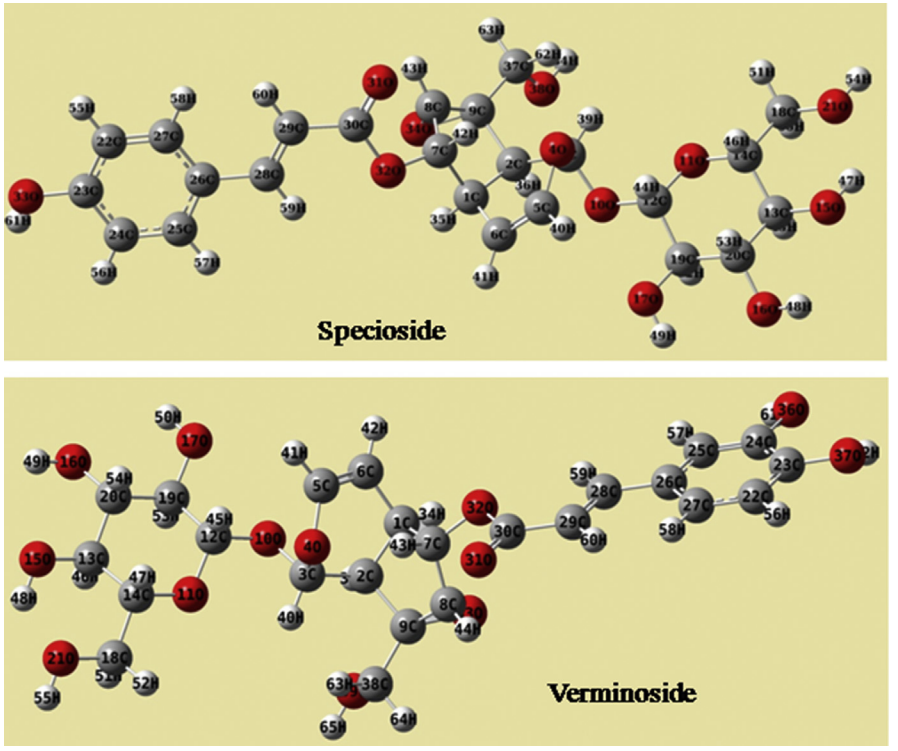

Fig. 2. The optimized structures of Specioside (SS) and Verminoside (VS).

https://doi.org/10.1016/j.heliyon.2019.e01118

2. Experimental

2.1. General

The Infrared (IR) spectrum of specioside (SS) and verminoside (VS) has done with the Perkin-Elmer FTIR spectrophotometer. ^{1}H and ^{13}C NMR spectrum were recorded on Bruker 300 MHz instrument using $CDCl_3$ solvent. Chemical shifts are reported in parts per million (ppm) using Tetramethylsilane (TMS) as internal standard. Ultra violet (UV) spectrum was recorded on UV−Visible Double-Beam Spectrophotometer instrument using $CHCl_3$ as a solvent. Melting point was determined by melting point apparatus. The thin layer chromatography (TLCs) was visualized in an iodine chamber.

2.2. Computational methods

The theoretical calculations of these compounds have been done with Gaussian 03 program package [16] and Gaussian 09 program package [17]. The results were examined with the Gaussview 03 molecular visualization program [18] and Gaussview 5.0 molecular visualization program [19]. Optimized geometrical parameters and vibrational frequencies for the compounds were calculated using DFT with a hybrid functional B3LYP [20] and basis set 6-31G (d,p). B3LYP invokes Becke's three parameter (local, non-local, Hartree-Fock) hybrid exchange functional (B3), with Lee−Yang−Parr correlation functional (LYP) [21]. The basis set 6-31G (d,p) with 'd' polarization functions on heavy atoms and 'p' polarization functions on hydrogen atoms is used for better description of polar bonds of molecule [22, 23]. It should be emphasized that 'p' polarization functions on hydrogen atoms are used for reproducing the out of plane vibrations involving hydrogen atoms. NMR chemical shifts were calculated with gauge including atomic orbital (GIAO) method using same level of theory [24]. In NBO basis, the second-order Fock matrix was used to estimate the donor−acceptor interactions [25]. By using Time Dependent Density Functional Theory (TDDFT) method, UV−Vis spectra, electronic transitions, and electronic properties like HOMO−LUMO energies were calculated.

Quantum chemical methods have been used to determining the molecular structure as well as for explaining the electronic structure and reactivity [26]. The Natural Bond Orbital (NBO), molecular electrostatic potential (MESP), electronic absorption spectra, Mulliken atomic charges and global reactivity descriptors were also investigated. For non linear optical devices, the Non Linear Optical (NLO) properties of the compound have also been studied revealing that the molecule is an attractive object for future studies of nonlinear optical properties as well as in pharmaceutical chemistry. The thermodynamic properties were also calculated at different temperatures revealing the correlation between the standard heat capacities (C), entropies (S) and temperatures. Surface morphology has been studied with

https://doi.org/10.1016/j.heliyon.2019.e01118

scanning electron microscopy (SEM) method [27, 28, 29]. We have proposed a multiphilic chemical reactivity descriptors calculated with the help of Fukui functions (FF) by DFT study. The explanation of the nucleophilicity and electrophilicity of the given atomic sites in the molecule with the help of chemical reactivity descriptors using DFT. global chemical reactivity trends are explained chemical potential, global hardness, global softness, electronegativity and electrophilicity. Fukui function (FF) and local softness is broadly applied for investigation of the local reactivity and site selectivity. The different applications of both global and local reactivity descriptors in the concern of chemical reactivity and site selectivity have been explained in detail. The definitions of all these descriptors and working equations for their computation have been described [20, 22, 30, 31]. Thus, to the best of our knowledge, this is the first time; a structural study of both the compounds has been done with compare to theoretical studies using density functional theory (DFT).

3. Result and discussion

3.1. ^{1}H NMR and ^{13}C NMR spectroscopy

Theoretical calculations of both the compounds were carried out using B3LYP/6-31G method. Chemical shifts were calculated with GIAO approach using B3LYP functional and 6-31G (d,p) basis set. The difference between isotropic magnetic shielding (IMS) of TMS and 'X' proton helps to find the chemical shift of any 'X' proton (CSX) and equation is given by CSX = IMSTMS -IMSX. The experimental and calculated values of ^{1}H NMR and ^{13}C NMR chemical shifts of the two compounds are shown in Table 1 [32−34]. The correlation graphs follow the linear equation, $y = 0.9489x + 0.4534$ using B3LYP for ^{1}H NMR and $y = 0.9703x + 16.03$ using B3LYP and for ^{13}C NMR where 'y' is the ^{1}H NMR and ^{13}C NMR experimental chemical shift and 'x' is the calculated ^{1}H NMR and ^{13}C NMR chemical shift (in ppm) and are shown in Figs. 3 and 4 respectively.

3.2. UV-Vis spectroscopy

Theoretical calculations of UV−Vis absorption spectrum were done with the help of TD-DFT method using B3LYP functional and 6-31G (d,p) basis set and solvent effect has been taken into consideration by implementing Integral Equation Formalism Polarizable Continuum Model (IEFPCM) Fig. 5. According to the frontier molecular orbital theory, the interaction between the HOMO and LUMO levels helps in chemical reactivity of reacting species [35]. The energy of the highest occupied molecular orbital (E_{HOMO}) measures the tendency towards the donation of electron by a molecule and higher values indicate good tendency towards the donation of electron. E_{LUMO} indicates the ability of the molecule to accept electrons. High value of E_{HOMO} is likely to a tendency of the molecule to donate electrons to appropriate

https://doi.org/10.1016/j.heliyon.2019.e01118

Table 1. Experimental and calculated ^{1}H NMR and ^{13}C NMR chemical shifts of Specioside (SS) and Verminoside (VS) compounds using DFT/B3LYP/6-31G (d, p) level.

Atom no.	^{1}H NMR Calculated B3LYP		^{1}H NMR Experimental		Atom no.	^{13}C NMR Calculated B3LYP		^{13}C NMR Experimental	
	SS	VS	SS	VS		SS	VS	SS	VS
H39	5.71		5.16	-	C3	98.18	98.12	95.20	95.20
H40	6.60	5.74	6.36	5.21	C5	142.82	143.06	142.50	142.50
H41	5.72	6.65	5.01	6.38	C6	112.11	112.19	103.00	103.00
H34	-	2.62		2.64					
H35	2.63	3.01	2.63	2.67	C1	40.10	39.67	36.80	36.90
H42	4.77	5.79	5.04	5.02	C7	88.87	88.41	78.10	81.40
H43	3.63	4.81	3.40	5.07	C8	63.34	63.08	65.80	81.40
H36	3.09	-	2.67	-	C9	70.45	70.44	66.90	66.90
H62	4.68	-	4.19	-	C2	52.91	52.93	42.20	43.30
H63	3.61	4.75	3.86	4.23	C37	66.90	-	61.40	-
H64	-	3.62		3.90	C38	-	66.44	-	61.4
H44	4.92	3.64	4.83	3.73	C12	101.27	101.11	99.80	99.8
H52	3.44	4.24	3.33 3.95	3.70	C19	75.74	75.76	74.90	74.9
H53	3.51	3.42	3.33 3.95	3.43−3.99	C20	81.63	81.51	81.40	78.5
H54	-	3.55	-	3.43−3.99					
H45	3.49	4.95	3.33 3.95	4.83	C13	79.63	79.59	71.80	71.9
H46	3.46	3.51	3.33 3.95	3.43−3.99	C14	75.16	75.16	78.70	77.8
H47	-	3.49		3.43−3.99					
H50	3.85	-	3.95	-	C18	71.38	71.17	63.00	63.0
H51	4.20	H51	3.70	3.97	C26	125.39	124.94	136.50	127.7
H58	7.94	7.59	7.48	6.83	C25	133.98	117.60	131.40	115.3
H55	7.00	-	6.81	-	C24	112.66	141.21	117.00	146.9
H56	6.67	6.99	6.81	7.02	C23	156.44	146.16	161.1	149.9
H57	6.78	6.71	7.48	7.11	C22	114.30	114.02	117.00	114.6
H59	7.54	6.14	7.66	7.66	C27	125.93	118.32	131.40	116.6
H60	6.13	4.51	6.38	6.38	C28	143.99	144.63	147.30	147.7
					C29	112.44	112.30	114.60	123.2
					C30	162.83	163.00	169.10	169.0

acceptor molecule of low empty molecular orbital energy [36]. Therefore, the energy of the HOMO is directly related to the ionization potential and LUMO energy is to the electron affinity. The difference of energies between HOMO and LUMO orbital is called as energy gap which is an important stability for the structures [37, 38, 39].

https://doi.org/10.1016/j.heliyon.2019.e01118

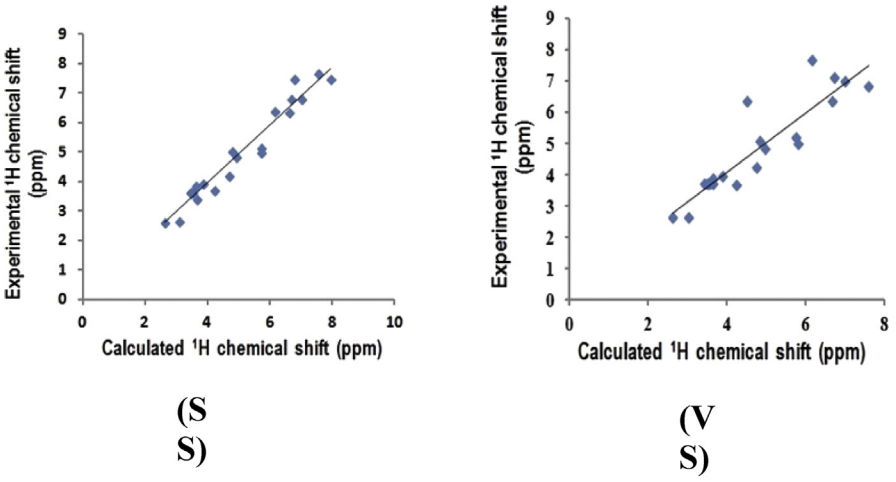

(SS) (VS)

Fig. 3. Correlation graph between experimental and calculated ^{1}H NMR chemical shift of Specioside (SS) and Verminoside (VS) using B3LYP/6-31G (d, p).

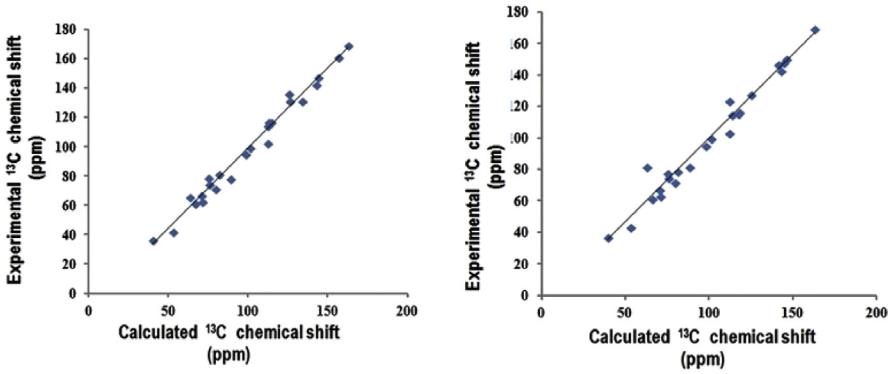

(SS) (VS)

Fig. 4. Correlation graph between experimental and calculated ^{13}C NMR chemical shift of Specioside (SS) and Verminoside (VS) using B3LYP/6-31G (d, p).

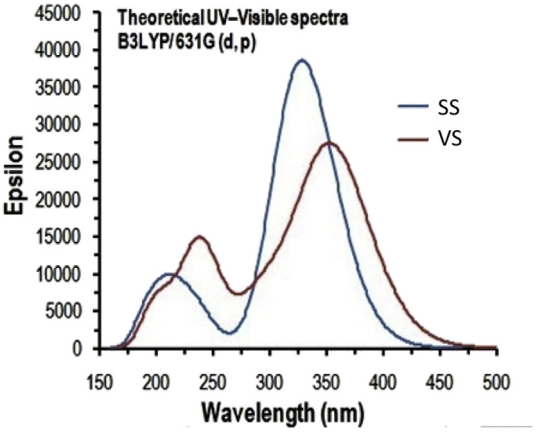

Fig. 5. Theoretical UV−Visible spectrum of Specioside (SS) and Verminoside (VS).

https://doi.org/10.1016/j.heliyon.2019.e01118

Calculations by B3LYP functional predict one intense electronic transition as good agreement with the measured experimental data as shown below. The transitions of both the compounds appear to be due to n → π*. Experimental and theoretical absorption wavelength and excitation energies of compounds are shown in Table 2. Molecular orbitals and their electronic transitions which show the distributions and different energy levels of the HOMO and LUMO orbitals at the B3LYP/6-31G(d, p) level for the specioside (SS) and verminoside (VS) compounds are shown in Fig. 5. Both the highest occupied molecular orbital (HOMO) and lowest unoccupied molecular orbital (LUMO) are the main orbital taking part in chemical stability. 3-Dimensional plots of highest occupied molecular orbitals (HOMOs) and lowest unoccupied molecular orbitals (LUMOs) of isolated compounds are shown in Fig. 6.

3.3. Vibrational assignment

The observed infrared and calculated wavenumbers, assignments and the calculated vibrational wavenumbers are different than the experimental wavenumbers due to discard of anharmonicity present in real system [40, 41]. Therefore, calculated wavenumbers are scaled down by a single factor 0.9679 for B3LYP and compared with experimental wavenumbers. The value of correlation coefficient (R2 = 0.9995 using B3LYP) showed that there is a good agreement between experimental and calculated wavenumbers [42, 43]. In specioside (SS), O-H stretching was observed at 3400 cm^{-1} and the calculated peaks found at 3607.92 cm^{-1} showing a better agreement with the experimental value. C=O Stretching frequency is normally found at above 1700 cm^{-1} but calculated peak was observed at 1724.20 cm^{-1}. C=C Stretching band observed experimentally at 1631cm^{-1} whereas calculated band observed at 1613.16 cm^{-1}. CH_2 in plane bending observed at 1475 cm^{-1} in experimental and calculated band

Table 2. Experimental and theoretical absorption wavelength λ (nm), excitation energies E (eV) of Specioside (SS) and Verminoside (VS) using B3LYP functional and 631-G/(d, p) basis set.

S.No.	Electronic transitions (MO involved)		Energy (eV)	Calculated λmax (nm) B3LYP	Oscillatory strength (f)	% contribution of probable transition B3LYP	Observed λmax (nm)
1.	SS	H-1→L H → L	4.57960 4.26831	300.98	0.1055	1.11	300
	VS	H-2→L H→L	5.01825 4.0427	329.88	0.6583	43.33	300
2.	SS	H-10→L H→ L+3	6.21362 6.68546	215.09	0.1593	2.53	245
	VS	H-10→L H-4→L H-2→L H-2→L+ H-3→L+1	6.0752 5.5570 5.0182 7.5137 5.6830	238.08	0.3159	9.97	253

https://doi.org/10.1016/j.heliyon.2019.e01118

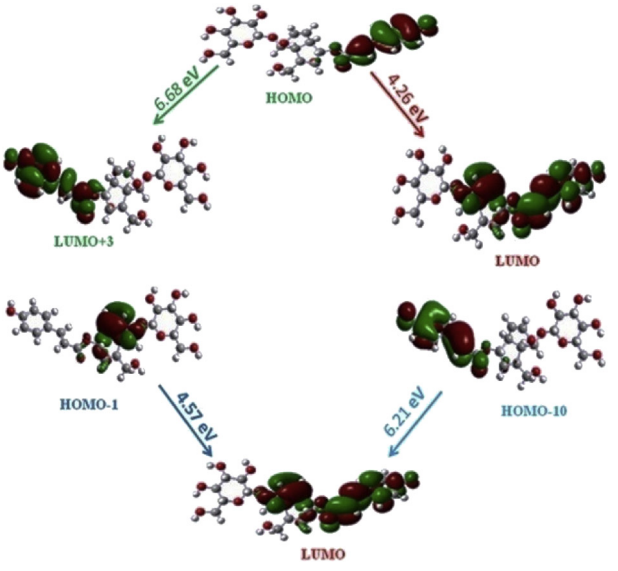

(SS)

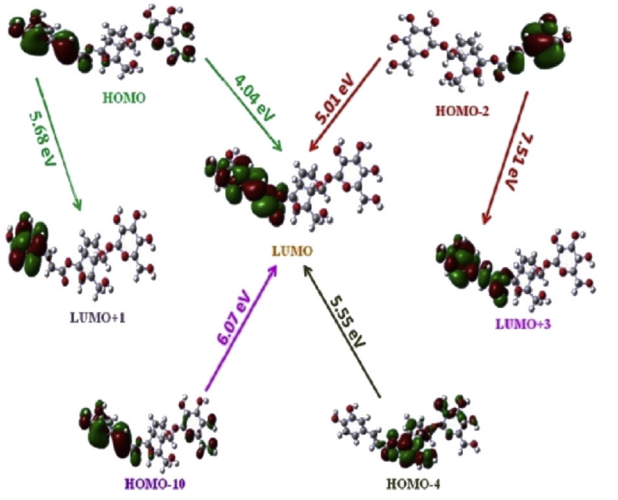

(VS)

Fig. 6. Molecular orbitals of the Specioside (SS) and Verminoside (VS) compound at the B3LYP/6-31G(d, p) basis set.

observed at 1400.58 cm^{-1}. C-C Stretching band value observed at 1550 cm^{-1} in experimental whereas calculated band observed at 1530.28 cm^{-1}. Therefore, the results have shown better agreement with the experimental values [44, 45, 46, 47, 48]. In verminoside (VS), O-H stretching band observed at 3340 cm^{-1} and the calculated band found at 3608.24 cm^{-1} thus showing better agreement with the experimental value. C=O Stretching frequency is normally found at above 1710 cm^{-1} but calculated peak observed at 1724.71 cm^{-1}, C=C stretching band observed at 1655 cm^{-1} and

https://doi.org/10.1016/j.heliyon.2019.e01118

1615 cm^{-1} in experimental whereas calculated band observed at 1593.28 cm^{-1} and 1524.92 cm^{-1}, CH_2 in plane bending observed at 1500 cm^{-1} in experimental and calculated peaks observed at 1475.09 cm^{-1}, C-C stretching band in experimental value 1498 cm^{-1} whereas in calculated band observed at 1438.21 cm^{-1}. Here, all results showed better agreement with the experimental values. In addition, both the bioactive compounds showed approximate similar IR bands (Table 3). The correlation graph between experimental and calculated vibrational frequencies of specioside (SS) and verminoside (VS) are shown in Fig. 7.

3.4. Molecular electrostatic potential

The electron density is of great significance factor related to the reactivity of electrophilic and nucleophilic sites and the interactions of hydrogen bonding as well as this density concerned to the molecular electrostatic potential (MESP). The importance of MESP lies in the fact that it simultaneously displays molecular size, shape as well as positive, negative and neutral electrostatic potential regions in terms of colour grading and is very useful in the investigation of molecular structure with its physiochemical property relationship [20, 49]. It helps to determine the reactivity of nucleophilic and electrophilic attack sites for compounds under study which simulated the MESP using the B3LYP level of the optimized geometry using Gauss view software as shown in Fig. 8. The red and blue region refers to the electron

Table 3. Experimental FT-IR and calculated vibrational frequencies in cm^{-1} for Specioside (SS) and Verminoside (VS).

Experimental	Calculated B3LYP		Vibrational assignment	
	SS	VS	SS	VS
3340	-	3608.24		O-H stretching
3400	3607.92	-	O-H stretching	-
1710	1724.20	1724.71	C=O stretching	C=O stretching
1655	-	1593.28	-	C=C stretching
1615	-	1524.92	-	C=C stretching
1631	1613.16		C=C stretching	-
1525	-	1475.09	-	CH_2 in plane bending (Scissoring)
1550	1530.28	-	C-C stretching	-
1475	1400.58	-	CH_2 in plane bending (Scissoring)	-
1498	-	1438.21	-	C-C stretching
3227	3267.7	-	=C-H stretching	-
3206	-	3198.24	-	=C-H stretching
2983	2986.69	-	-C-H stretching	-
2984	-	2976.6	-	-C-H stretching

https://doi.org/10.1016/j.heliyon.2019.e01118

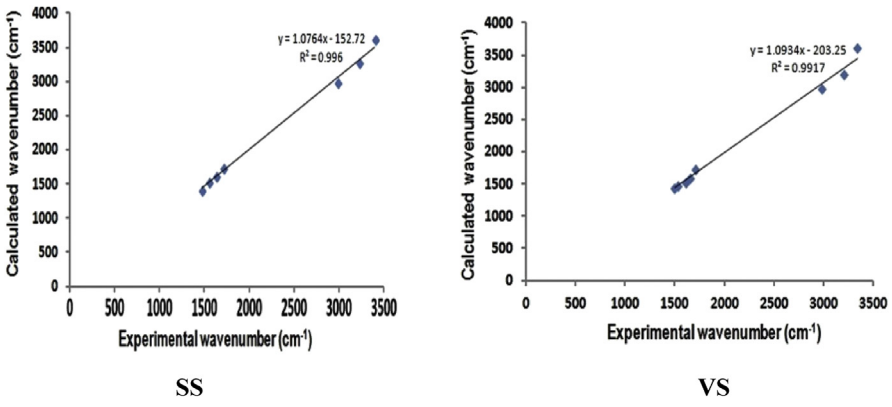

Fig. 7. Experimental FT-IR and calculated vibrational frequencies in cm^{-1} of Specioside (SS) and Verminoside (VS).

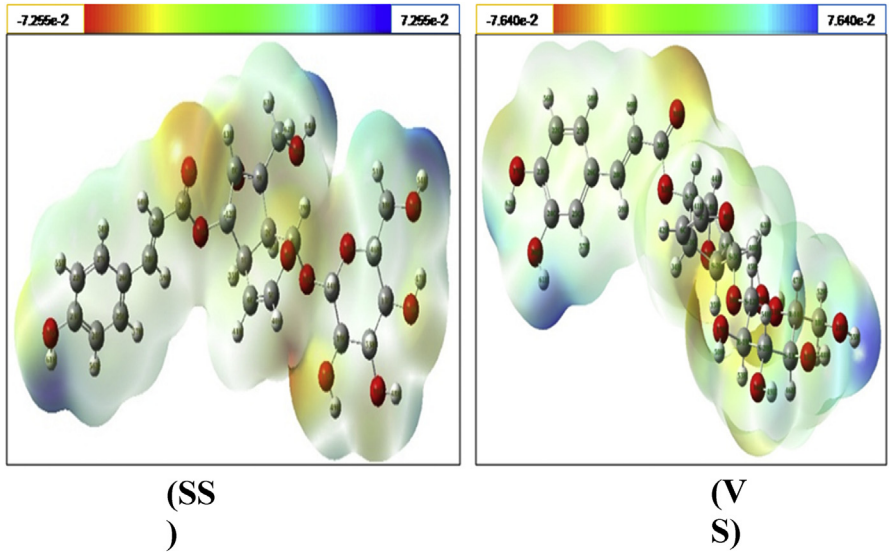

Fig. 8. 3D plots of the molecular electrostatic potential of Specioside (SS) and Verminoside (VS).

rich means electrophilic attack and electron poor means nucleophilic attack region while green region shows the neutral region [50]. MESP of both compounds showed the major negative potential region around oxygen atoms of alcoholic group indicating the binding site for nucleophilic attack [51, 52].

3.5. Natural bond orbital analysis (NBO)

The NBO calculated hybridizations is of great significant parameters for our structure analysis. It was determined by using the Gaussian 03 package at the B3LYP/6-31G (d,p) method. Gaussian software helps to calculate bond length and bond angles values for the compounds. Natural Bond Orbital's are localized few-center orbitals explain the Lewis-like molecular bonding pattern in compact form of electron

https://doi.org/10.1016/j.heliyon.2019.e01118

pairs. NBOs are localized "maximum occupancy" orbital's whose leading N/2 members (or N members in the open-shell case) and Lewis-like description of the total N-electron density. Second-order perturbation theory indicates that all possible interactions are analysed between "filled" (donor) Lewis-type NBOs and "empty" (acceptor) non-Lewis NBOs. Evaluation of NBO analysis helps to evaluate interaction between donor (i) level bonds donor-acceptor (j) level bonds. The result of interaction is a loss of occupancy from the concentration of electron NBO of the idealized Lewis structure into an empty non-Lewis orbital [53, 54]. For each donor (i) and acceptor (j) the stabilization energy E(2) concerned with the delocalization i → j is as follows:

$$E(2) = \Delta Eij = qi(Fij)^2 / (Ej - Ei) \quad (1)$$

i.e. qi is the donor orbital occupancy, Ei and Ej are the diagonal elements and Fij is the of diagonal NBO Fock matrix element. The large E(2) value exhibits the intensive interaction between electron-donors and electron-acceptors and the extent of conjugation of the whole system of both the compounds that are given in NBO Tables 4 and 5 respectively. Stabilization of the system was observed of the following strong intramolecular hyperconjugative interactions causing increased electron density (ED) and intramolecular charge transfer (ICT) [55]. The elongation and red shift provided the knowledge of the electron density of n(O) is transferred to π*, σ* (antibonding orbitals) of C- C, C-O and O-C bonds.

Specioside (SS)

Between n_2 (O_{31}) → σ*(C_{30}-O_{32}) which increases ED (0.62 e) leading to stabilization of 34.28 kcal mol^{-1}.

Between n_2 (O_{32}) → π^* (C_{30}-O_{31}) which increases ED (0.33 e) leading to stabilization of 45.82 kcal mol^{-1}.

Between n_2 (O_{33}) → π^* (C_{23}-C_{24}) which increases ED (0.35 e) leading to stabilization of 30.42 kcal mol^{-1}.

Between C_{23}-C_{24} from π→π* (C_{22}-C_{27}) which increases ED (0.01 e) leading to stabilization of 209.97 kcal mol^{-1}

Between C_{23}-C_{24} from π→π* (C_{25}-C_{26}) which increases ED (0.01 e) leading to stabilization of 291.45 kcal mol^{-1}

Between C_{23}-C_{24} from π→π* (C_{25}-C_{26}) which increases ED (0.01 e) leading to stabilization of 291.45 kcal mol^{-1}

Between C_{25}-C_{26} from π→π* (C_{28}-C_{29}) which increases ED (0.02 e) leading to stabilization of 89.50 kcal mol^{-1}

Between C_{30}-O_{31} from π→π* (C_{28}-O_{29}) which increases ED (0.03 e) leading to stabilization of 48.76 kcal mol^{-1}

https://doi.org/10.1016/j.heliyon.2019.e01118

Table 4. Second order perturbation theory analysis of Fock matrix in NBO basis of Specioside (SS).

Donor(i)	Type	ED/e	Acceptor(j)	Type	ED/e	E(2)[a]	E(j) _ E(i)[b]	F(i,j)[c]
C22 - C27	π	1.71369	C23 - C24	π^*	0.39067	22.41	0.28	0.072
C22 - C27	π	1.71369	C25 - C26	π^*	0.38809	16.09	1.07	0.062
C23 - C24	π	1.64293	C22 - C27	π^*	0.29065	15.21	0.30	0.061
C23 - C24	π	1.64293	C25 - C26	π^*	0.38809	23.27	0.29	0.074
C25 - C26	π	1.63048	C22 - C27	π^*	0.29065	20.87	0.28	0.070
C25 - C26	π	1.63048	C23 - C24	π^*	0.39067	18.04	0.27	0.062
C25 - C26	π	1.63048	C28 - C29	π^*	0.12257	17.75	0.29	0.069
C28 -C29	π	1.85559	C25 - C26	π^*	0.38809	11.08	0.30	0.055
C28 -C29	π	1.85559	C30 - O31	π^*	0.27828	22.11	0.29	0.073
LP (2) O4	n	1.86104	C3 - O10	σ^*	0.05778	12.87	0.62	0.081
LP (2) O4	n	1.86104	C5 - C6	π^*	0.10538	19.54	0.38	0.077
LP (2) O10	n	1.87748	C3 - O4	σ^*	0.06492	12.94	0.58	0.078
LP (2) O10	n	1.87748	O11 - C12	σ^*	0.06032	15.20	0.58	0.085
LP (2) O31	n	1.85245	C29 - C30	σ^*	0.05242	17.06	0.71	0.100
LP (2) O31	n	1.85245	C30 - O32	σ^*	0.10561	34.28	0.62	0.132
LP (2) O32	n	1.80480	C30 - O 31	π^*	0.27828	45.82	0.33	0.112
LP (2) O33	n	1.86065	C23 - C24	π^*	0.39067	30.42	0.35	0.098
C23 - C24	π	0.39067	C22 - C27	π^*	0.29065	209.97	0.01	0.082
C23 - C24	π	0.39067	C25 - C26	π^*	0.38809	291.45	0.01	0.080
C25 - C26	π	0.38809	C28 - C29	π^*	0.12257	89.50	0.02	0.066
C30 - O31	π	0.27828	C28 - C29	π^*	0.12257	48.76	0.03	0.073

[a] E (2) means energy of hyper conjugative interactions (stabilization energy in Kcal/mol).
[b] Energy difference between donor and acceptor i and j NBO orbitals in a. u.
[c] F (ij) is the Fock matrix elements between i and j NBO orbitals in a. u.

Verminoside (VS)

Between n_2 (O_{31}) → σ* (C_{30}-O_{32}) which increases ED (0.62 e) leading to stabilization of 34.34 kcal mol^{-1}.

Between n_2 (O_{32}) → π^* (C_{30}-O_{31}) which increases ED (0.33 e) leading to stabilization of 45.68 kcal mol^{-1}.

Between n_2 (O_{32}) → π^* (C_{30}-O_{31}) which increases ED (0.33 e) leading to stabilization of 45.68 kcal mol^{-1}.

Between C_{24}-C_{25} from σ→ π^* (C_{26}-C_{27}) which increases ED (0.01 e) leading to stabilization of 258.48 kcal mol^{-1}

Between C_{26}-C_{27} from σ→ π^* (C_{28}-C_{29}) which increases ED (0.01 e) leading to stabilization of 153.71 kcal mol^{-1}

https://doi.org/10.1016/j.heliyon.2019.e01118

Table 5. Second order perturbation theory analysis of Fock matrix in NBO basis of the Verminoside (VS).

Donor(i)	Type	ED/e	Acceptor(j)	Type	ED/e	E(2)[a]	E(j)_E(i)[b]	F(i,j)[c]
C22 - C23	σ	1.97463	C24 - C25	σ^*	0.02261	19.99	0.28	0.067
C22 - C23	σ	1.97463	C26 - C27	σ^*	0.02383	21.52	0.29	0.072
C24 -C25	σ	1.71181	C22 -C23	σ^*	0.39246	18.48	0.30	0.068
C24 -C25	σ	1.71181	C26 -C27	σ^*	0.40814	16.67	0.31	0.066
C26 -C27	σ	1.63286	C22 -C23	σ^*	0.39246	19.98	0.27	0.066
C26 -C27	σ	1.63286	C24 -C25	σ^*	0.38095	20.33	0.27	0.066
C26 -C27	σ	1.63286	C28 -C29	π^*	0.12404	14.32	0.29	0.061
C28 -C29	π	1.85501	C26-C27	σ^*	0.40814	10.38	0.30	0.054
C28 -C29	π	1.85501	C30-O31	π^*	0.27877	22.10	0.29	0.073
LP(2)O4	n	1.86161	C5 - C6	π^*	0.10466	19.23	0.38	0.077
LP(2)O10	n	1.87718	C3 - O4	σ^*	0.06500	12.95	0.58	0.078
LP(2)O10	n	1.87718	O11 -C12	σ^*	0.06022	15.16	0.58	0.085
LP(2)O31	n	1.85217	C29 -C30	σ^*	0.05229	17.04	0.71	0.100
LP(2)O31	n	1.85217	C30 -O32	σ^*	0.10588	34.34	0.62	0.132
LP(2)O32	n	1.80525	C30 -O31	π^*	0.01820	45.68	0.33	0.112
LP(2)O36	n	1.89312	C24-C25	σ^*	0.38095	25.47	0.36	0.092
LP(2)O37	n	1.85621	C22-C23	σ^*	0.39246	29.76	0.34	0.096
C24 -C25	σ	0.38095	C26-C27	σ^*	0.40814	258.48	0.01	0.079
C26 -C27	σ	0.40814	C28-C29	π^*	0.12404	153.71	0.01	0.073
C30 -O31	π	0.27877	C28-C29	π^*	0.12404	49.58	0.03	0.073

[a] E (2) means energy of hyper conjugative interactions (stabilization energy in Kcal/mol).

[b] Energy difference between donor and acceptor i and j NBO orbitals in a. u.

[c] F (ij) is the Fock matrix elements between i and j NBO orbitals in a. u.

3.6. Non linear optical analysis (NLO)

The Non-Linear Optical (NLO) parameters of the compounds have been calculated by using B3LYP levels with 6-31G (d, p) basis set. It deals with the interaction of applied electromagnetic fields in various materials to generate new electromagnetic fields, altered in wave number, phase, or other physical properties. Organic molecules able to manipulate photonic signals efficiently are of importance in technologies such as optical communication, optical computing, and dynamic image processing [56, 57, 58]. Mainly polarizability and hyperpolarizability are important parameters to determine the structural chemistry and efficiency of the polarizability and hyperpolarizability properties of molecular systems depend on the charge transfer between electron donating and withdrawing groups that helps in determining the intramolecular charge transfer. The intermolecular interactions involving the non-bonded type dipole−dipole interactions are determined with the help of dipole moment of a molecule means stronger the dipole moment, stronger will be the

https://doi.org/10.1016/j.heliyon.2019.e01118

intermolecular interactions. The first hyperpolarizability is a third rank tensor that can be described by a 3 × 3 × 3 matrix. In theory of Kleinman symmetry, 27 components of the matrix can be reduced to 10 components. The complete equations for calculating the magnitude of total dipole moment μ, the average polarizability α_{tot} and the first hyperpolarizability β_{tot}, using the x,y,z components is as follows:

$$\mu_{tot} = \left(\mu_x^2 + \mu_y^2 + \mu_z^2\right)^{1/2} \tag{2}$$

$$\alpha_{tot} = 1/3\left(\alpha_{xx} + \alpha_{yy} + \alpha_{zz}\right) \tag{3}$$

$$< \beta >= \left[\left(\beta_{xxx} + \beta_{xyy} + \beta_{xzz}\right)^2 + \left[\left(\beta_{yyy} + \beta_{yzz} + \beta_{yxx}\right)^2 + \left[\left(\beta_{zzz} + \beta_{zxx} + \beta_{zyy}\right)^2\right]^{1/2} \tag{4}$$

Since the value of the polarizabilities α and the hyperpolarizability of Gaussion output are reported in a atomic mass units (a.m.u.), the calculated values have been converted into electrostatic units (esu) (α: 1 a.u = 0.1482×10^{-24} esu; β: 1 a.m.u. = $.0086393\times10^{-30}$ esu). The results of electronic dipole moment μi (i = x, y, z), polarizability αij and first order hyperpolarizability βijk are shown in Table 6. The calculated dipole moment is equal to 2.6733 D for B3LYP level. The calculated polarizability α_{tot},of specioside (SS) is equal to 303.15 $\times10^{-24}$ esu and verminoside (VS) is eequal to 308.82×10^{-24} esu for B3LYP level as shown in Table 6. The calculated first hyper polarizability of the specioside (SS) is 55.8 $\times10^{-30}$ esu and verminoside (VS) is 3385.0111 for B3LYP level and these values

Table 6. Dipole moment μ, polarizability α_{tot} ($\times10^{-24}$esu) and first order static hyperpolarizability β(10^{-30}) data for Specioside (SS) and Verminoside (VS) calculated at DFT/B3LYP/6-31G(d, p) level of theory.

Dipole moment	**B3LYP**		**Hyperpolarizability**	**B3LYP**	
	SS	**VS**		**SS**	**VS**
μ_x	-2.0984	3.3997	β_{xxx}	-2169.83	2733.90
μ_y	-0.7682	-0.5940	β_{xxy}	-1001.80	-1102.94
μ_z	1.9686	2.3446	β_{xyy}	-355.917	358.031
$(\mu)_{tot}$	2.9779	4.1722	β_{yyy}	-199.675	-236.948
Polarizability					
α_{xx}	432.330	443.088	β_{xxz}	656.971	-609.150
α_{xy}	48.0998	-45.8625	β_{xyz}	138.708	111.227
α_{yy}	265.654	269.774	β_{yyz}	49.0201	-70.9699
α_{xz}	-16.5410	-11.4405	β_{xzz}	-107.113	85.3043
α_{yz}	-32.3129	31.0162	β_{yzz}	1.73262	-29.8434
α_{zz}	211.470	213.615	β_{zzz}	12.1332	-35.9025
$(\alpha)_{tot}$	303.1513	308.8256	$\beta_{total(esu)}$	55.8075	3385.0111

https://doi.org/10.1016/j.heliyon.2019.e01118

are 429 times greater in case of specioside (SS) and approximately more than 25000 times in case of verminoside (VS) for B3LYP level than that of the standard NLO material (0.13×10^{-30}esu) [59]. Both compounds, therefore, provide an attractive object for future studies of nonlinear optical properties.

3.7. Thermodynamic properties

The Thermodynamic parameters include zero-point vibrational energy, rotational temperatures, rotational constants and energies at standard temperature 298.15 K, were obtained at the HF and DFT using B3LYP functional with 631-G (d,p) basis set. At different temperatures (100−500 K), the vibrational analysis, values of standard statistical thermodynamic functions, heat capacity (CV) and entropy (S) were determined using DFT/B3LYP method with 6-31G (d, p) basis set. The higher values were calculated in HF of the total energy, translational, rotational, and vibrational energy than B3LYP. The rotational constants and rotational temperature values are similar in all the cases. It was observed that standard statistical thermodynamic functions increase with temperature ranging from 100 to 500 K, due to the fact that the molecular vibrational intensities increase with temperature [60]. The correlation equations among heat capacities, entropies and temperatures were fitted by quadratic formulas and the corresponding fitting factors (R^2) for these thermodynamic properties. The corresponding fitting equations and the correlation graphics (Figs. 9 and 10) are as follows.

$$CV = 3.838 + 0.145T - 1.10^{-4}T^2\left(R^2 = 0.981\right) \tag{5}$$

$$S = 67.037 + 0.4242T - 0.0001T^2\left(R^2 = 0.951\right) \tag{6}$$

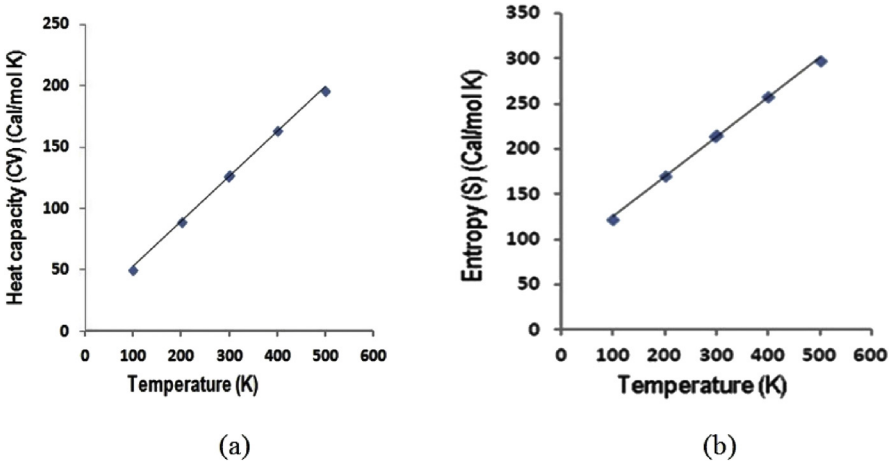

Fig. 9. Correlation graphs of Heat Capacity (a) and Entropy (b) calculated at various temperatures of Specioside (SS) using B3LYP/6-31G(d, p) basis set.

https://doi.org/10.1016/j.heliyon.2019.e01118

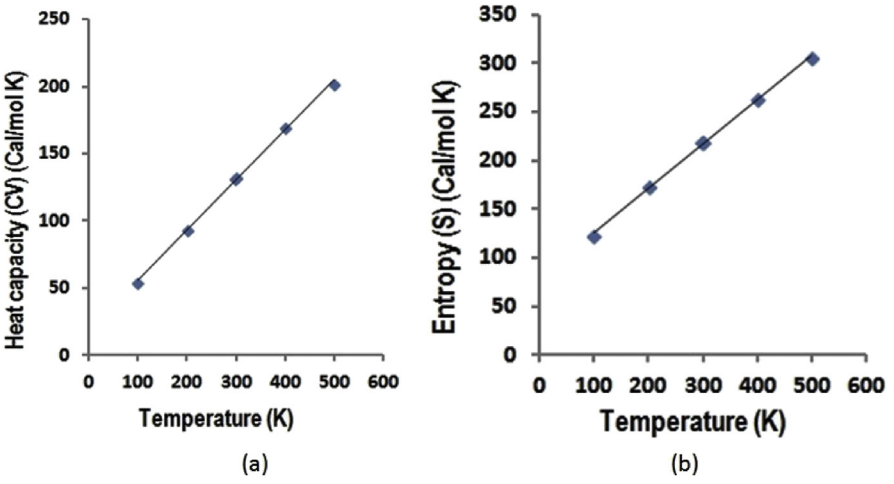

Fig. 10. Correlation graphs of Heat Capacity (a) and Entropy (b) calculated at various temperatures of Verminoside (VS) using B3LYP/6-31G(d, p) basis set.

According to the second law of thermodynamics in thermochemical field, these thermodynamic data provide helpful information for the study of compounds to compute the other thermodynamic energies in relation of thermodynamic functions and estimate directions of chemical reactions. All thermodynamic calculations were done in gas phase but not used in solution (Tables 7 and 8).

3.8. Chemical reactivity descriptors

Global reactivity descriptors (GRDs) determine the nature of many of the basic chemical concepts like hardness and softness and justified framework of the DFT [29, 61]. GRDs are highly successful in predicting global reactivity trends. According to the Koopman's theorem, the energies of frontier molecular orbital (εLUMO,

Table 7. Calculated thermodynamic parameters of Specioside (SS) and Verminoside (VS).

Parameters		B3LYP 6−31, G (d, p)	
		SS	VS
Zero point vibrational Energy (kcal/mol)		320.43186	322.87109
Rotational temperature (K)		0.01229	0.01150
		0.00158	0.00145
		0.00147	0.00136
Rotational constant (GHZ)			
	X	0.25610	0.23972
	Y	0.03286	0.03022
	Z	0.03064	0.02835
Total energy Etotal (kcal/mol)		340.971	344.317
	Translational	0.889	0.889
	Rotational	0.889	0.889
	Vibrational	339.194	342.540

https://doi.org/10.1016/j.heliyon.2019.e01118

Table 8. Thermodynamic functions at different temperatures at the B3LYP/6-31G (d, p) level of Specioside (SS) and Verminoside (VS).

Temperature (T) (K)	Heat capacity (CV) (Cal/mol K) B3LYP 6-31G (d, p)		Entropy (S) (Cal/mol K) B3LYP 6-31G (d, p)	
	SS	VS	SS	VS
100	50.936	53.424	122.312	122.981
200	89.106	93.376	170.892	173.929
298.150	126.633	131.552	214.217	219.102
300	127.345	132.272	215.015	219.931
400	164.282	169.461	257.373	263.746
500	195.852	201.164	297.983	305.526

εHOMO), band gap (εLUMO - εHOMO), ionization potential(IP), electron affinity (EA) [62], electronegativity (χ), global hardness(η) [63], chemical potential (l), global electrophilicity index (x), global softness (*S*) and additional electronic charge (ΔN_{max}) of compounds have been calculated are as follows:

$$IP = -\varepsilon_{HOMO} \tag{7}$$

$$EA = -\varepsilon_{LUMO} \tag{8}$$

$$\chi = -1/2(\varepsilon_{LUMO} + \varepsilon_{HOMO}) \tag{9}$$

$$\eta = 1/2(\varepsilon_{LUMO} - \varepsilon_{HOMO}) \tag{10}$$

$$\mu = -\chi = 1/2(\varepsilon_{LUMO} + \varepsilon_{HOMO}) \tag{11}$$

$$\omega = \mu^2/2\eta \tag{12}$$

$$S = 1/2\eta \tag{13}$$

$$\Delta N_{\max} = -\mu/\eta \tag{14}$$

Electrophilicity index (ω) is a global reactivity index similar to the chemical hardness and chemical potential introduced by Parr *et al* [64]. The maximum charge transfer ΔN_{max} towards the electrophile was evaluated showing the property of the system to acquire additional electronic charge from the environment which describes the charge capacity of the molecule. This new reactivity index measures the stabilization in energy when the system acquires an additional electronic charge (ΔN) from the environment [30, 65, 66, 67]. The direction of the charge transfer is completely determined by the electronic chemical potential of the molecule because an electrophile is a chemical species capable of accepting electrons from

https://doi.org/10.1016/j.heliyon.2019.e01118

the environment. Therefore its energy must decrease upon accepting electronic charge and its electronic chemical potential must be negative (Table 9).

3.9. Local reactivity descriptors

Fukui Function (FF) is most widely used for local density functional descriptors to model chemical reactivity and site selectivity [68]. The atom is highly reactive compared to the other atoms in the molecule with the high FF. Using Hirshfeld population analysis of neutral, cation and anion state of molecule, Fukui functions are calculated using following equations:

$$f_k^+ = [q(N+1) - q(N)] \text{ for nucleophilic attack} \quad (15)$$

$$f_k^- = [q(N) - q(N-1)] \text{ for electrophilic attack} \quad (16)$$

$$f_k^0 = 1/2[q(N+1) - q(N-1)] \text{ for radical attack} \quad (17)$$

where N, N-1, N+1 are total electrons present in neutral, anion and cation state of molecule respectively. In addition local softnesses ($S_k{}^+$, $S_k{}^-$, $S_k{}^0$) and electrophilicity indices ($\omega_k{}^+$, $\omega_k{}^-$, $\omega_k{}^0$) are also used to describe the reactivity of atoms in a molecule [69, 70]. These local reactivity descriptors associated with a site k in a molecule are defined with the help of the corresponding condensed to atom variants of Fukui function, using the following equations,

$$S_k^+ = Sf_k^+, S_k^- = Sf_k^-, S_k^0 = Sf_k^0 \quad (18)$$

$$\omega_k^+ = \omega f_k^+, \omega_k^- = \omega f_k^-, \omega_k^0 = \omega f_k^0 \quad (19)$$

where +, −, 0 signs show nucleophilic, electrophilic and radical attack respectively. The maximum values of all the three local reactivity descriptors ({$f_k{}^+$, $f_k{}^-$}; {$S_k{}^+$, $S_k{}^-$}; {$\omega_k{}^+$, $\omega_k{}^-$}) indicate that this is more occupied site for nucleophilic or electrophilic attack than all other atomic sites in reactants i.e. Fukui functions ($f_k{}^+$, $f_k{}^-$) local softnesses ($S_k{}^+$, $S_k{}^-$)and local electrophilicity indices ($\omega_k{}^+$, $\omega_{k)}$ for selected atomic sites of molecule [65, 71, 72].

Table 9. Calculated εLUMO, εHOMO, energy band gap εLUMO - εHOMO, ionization potential (IP), electron affinity (EA), electronegativity (χ), global hardness (η), chemical potential (μ), global electrophilicity index (ω), global softness (*S*) and additional electronic charge (ΔNmax) in eV for Specioside (SS) and Verminoside (VS) using B3LYP/6-31G (d, p) level.

Compound	ε_H	ε_L	ε_H -ε_L	I	A	χ	η	μ	ω	*S*	ΔN_{max}
SS	-0.021	-0.062	0.041	0.021	0.062	0.041	-0.02	-0.041	-24.92	-24.87	-2.05
VS	-0.211	-0.062	0.273	0.211	0.062	-0.74	0.151	0.74	1.813	3.311	-4.9

https://doi.org/10.1016/j.heliyon.2019.e01118

https://doi.org/10.1016/j.heliyon.2019.e01118

Table 10. Using Hirshfeld population analysis: Fukui functions (f_k^+, f_k^-), Local softnesses (Sk^+, Sk^-) in eV, local electrophilicity indices ($\omega\kappa+$, $\omega\kappa^-$) in eV for selected atomic sites of Specioside (SS).

Atom no.	Hirshfeld atomic Charges			Fukui functions		Local softnesses		Local electrophilicity indices	
	qN	qN + 1	qN − 1	f_k^+	f_k^-	Sk^+	Sk^-	ωκ+	ωk −
1C	-0.045469	-0.024876	-0.030297	0.020593	-0.015172	-0.512327	1.377459	-0.513228	1.378123
2C	0.014529	0.083650	0.042533	0.069121	-0.028004	-1.719641	1.696703	-1.722667	1.697929
3C	0.466198	0.515731	0.492852	0.049533	-0.026654	-1.232317	0.663117	-1.234485	0.664283
4O	-0.510039	-0.453766	-0.507813	0.056273	-0.002226	-1.399999	0.055380	-1.402463	0.055477
5C	0.339498	0.364176	0.243067	0.024678	0.096431	-0.613956	-2.399079	-0.615037	-2.4033
6C	-0.101690	0.063877	-0.001330	0.165567	-0.10036	-4.119094	2.496827	-4.126341	2.50122
7C	0.356028	0.330071	0.329753	-0.025957	0.026275	0.645776	-0.653688	0.646912	-0.654838
8C	0.187945	0.230416	0.210512	0.042471	-0.022567	-1.056623	0.561437	-1.058482	0.562425
9C	0.296323	0.223077	0.219396	-0.073246	0.076927	1.822266	-1.913844	1.825472	-1.917215
10O	-0.508178	-0.501064	-0.509083	0.007114	0.000905	-0.176987	-0.022515	-0.177298	-0.022554
11O	-0.500222	-0.528881	-0.529012	-0.028659	0.028659	0.712999	-0.712999	0.714253	-0.714253
12C	0.507592	0.526612	0.530941	0.01902	-0.023349	-0.473193	0.580893	-0.474025	0.113322
13C	0.244649	0.263851	0.249237	-0.00951	-0.004588	0.236596	0.114135	0.237012	0.114344
14C	0.289707	0.242805	0.244460	-0.046902	0.045247	1.166788	-1.125687	1.168914	-1.127667
15O	-0.226747	-0.235139	-0.264649	-0.008392	0.037902	1.208782	-0.942953	0.209149	-0.944612
16O	-0.244165	-0.235457	-0.257437	0.008708	0.501602	-0.216643	-12.479213	-0.217025	-12.501169
17O	-0.222951	-0.231618	-0.235913	-0.008667	0.012962	0.215623	-0.322477	0.216003	-0.323045
18C	0.184110	0.255803	0.244165	0.071693	-0.060055	-1.783629	1.494091	-1.786768	1.496719
19C	0.270268	0.269160	0.261067	-0.001108	0.009201	0.027565	-0.228909	0.027614	-0.229311
20C	0.232849	0.230962	0.219998	-0.001887	0.012851	0.046946	-0.319716	0.047028	-0.320278
21O	-0.217738	-0.221162	-0.237896	-0.003424	0.020158	0.085184	-0.501505	0.085334	-0.502387
22C	-0.026457	0.070269	-0.072353	0.096726	0.045896	-2.406418	-1.141833	-2.410652	-1.143842
23C	0.356361	0.356415	0.277465	0.000054	0.078896	-1.001343	-0.078896	-0.001345	-1.966284

(*continued on next page*)

Table 10. (*Continued*)

Atom no.	Hirshfeld atomic Charges			Fukui functions		Local softnesses		Local electrophilicity indices	
	qN	qN $^{+}$ 1	qN $^{-}$ 1	f_k^+	f_k^-	Sk^+	Sk^-	ωκ+	ωk $^{-}$
24C	-0.074666	0.021250	-0.131307	0.095916	0.056641	-2.386266	-1.409155	-2.390465	-1.411634
25C	-0.024286	0.018534	-0.118962	0.04282	0.094676	-1.065306	-2.355417	-1.06718	-2.359561
26C	0.147078	0.141424	0.136825	-0.005654	0.010253	1.140664	-1.255081	0.1409117	-0.25553
27C	0.009456	0.031452	-0.104278	-0.0063108	0.113734	1.157004	-2.829558	0.15728	-2.834534
28C	0.028443	0.066319	-0.122698	0.037876	0.151141	-1.942306	-3.760194	-0.943964	-3.766809
29C	-0.082786	0.016853	-0.180417	0.099639	0.097631	-2.478890	-2.428933	-2.483251	-2.433207
30C	0.659226	0.639428	0.548174	-0.019798	0.111052	0.492548	-2.762831	0.493415	-2.767692
31O	-0.528249	-0.469432	-0.609497	0.058817	-0.081248	-1.463291	2.021345	-1.465865	2.024902
32O	-0.520803	-0.503404	-0.519430	0.017399	-0.001373	-0.432864	0.034158	-0.433626	0.034218
33O	-0.226659	-0.142820	-0.300413	0.083839	0.073754	-2.085806	-1.834904	-2.089476	-1.838133
34O	-0.497902	-0.452460	-0.478219	0.950362	-0.019683	-23.643786	0.489687	-23.685384	0.490549
37C	0.173231	0.243645	0.193692	0.070414	-0.020461	-1.751809	1.509043	-1.754891	0.509939
38O	-0.204483	-0.205702	-0.233131	-0.001219	0.028648	0.030327	-1.712725	0.03038	-0.713979

https://doi.org/10.1016/j.heliyon.2019.e01118

https://doi.org/10.1016/j.heliyon.2019.e01118

Table 11. Using Hirshfeld population analysis: Fukui functions (f_k^+, f_k^-), Local softnesses (Sk^+, Sk^-) in eV, local electrophilicity indices ($\omega\kappa+$, $\omega\kappa^-$) in eV for selected atomic sites of Verminoside (VS).

Atom no.	Hirshfeld atomic Charges			Fukui functions		Local softnesses		Local electrophilicity indices	
	qN	qN + 1	qN − 1	f_k^+	f_k^-	Sk^+	Sk^-	$\omega\kappa+$	ωk^-
1C	-0.046135	-0.028520	-0.031922	0.017615	-0.014213	0.058323	-0.047059	0.031935	-0.025768
2C	0.014704	0.080005	0.039877	0.065301	-0.025173	0.216211	-0.083347	0.11839	-0.045638
3C	0.466207	0.517220	0.495390	0.051013	-0.029183	0.168904	-0.096624	0.052908	-0.052908
4O	-0.509963	-0.459482	-0.508047	0.050481	-0.001916	0.167142	-0.006343	0.091522	-0.003473
5C	0.340001	0.356908	0.243768	0.016907	0.096233	0.055979	0.3186274	0.030652	0.174470
6C	-0.101848	0.053355	-0.001955	0.155203	-0.099893	0.513877	-0.330745	0.281383	-0.181106
7C	0.356426	0.330155	0.330578	-0.026271	0.025848	-0.086983	0.085582	-0.047629	0.046862
8C	0.188006	0.227177	0.211029	0.039171	-0.023023	0.129695	-0.076229	0.071017	-0.04174
9C	0.296268	0.223178	0.218971	-0.07309	0.077297	-0.242	0.25593	-0.132512	0.140139
10O	-0.508225	-0.501495	-0.509003	0.00673	0.000778	0.022283	-.0025759	0.012201	0.00141
11O	-0.500298	-0.531596	-0.529806	-0.031298	0.029508	-0.103627	0.0977	-0.056743	0.053498
12C	0.507631	0.526467	0.531312	0.018836	-0.023681	0.059978	-0.078407	0.034149	-0.042933
13C	0.244680	0.262795	0.249345	0.018115	-0.004665	0.059978	-0.015445	0.032842	-0.008457
14C	0.289701	0.242527	0.245109	-0.047174	0.044592	-0.156193	0.147644	-0.085526	0.080845
15O	-0.226659	-0.239524	-0.264389	-0.011016	0.03773	-0.036473	0.124924	-0.019972	0.068404
16O	-0.244058	-0.237675	-0.257407	0.006383	0.013349	0.021134	0.044198	0.011572	0.038315
17O	-0.222998	-0.233957	-0.236213	-0.010959	0.013215	-0.036285	0.043754	-0.019868	0.023958
18C	0.184168	0.252994	0.243727	0.068826	-0.059559	0.227882	-0.197199	0.124781	-0.10798
19C	0.270302	0.268127	0.260953	-0.002175	0.009349	-0.007201	0.030954	-0.003943	0.016949
20C	0.232944	0.230039	0.220293	-0.002905	0.012651	-0.007201	0.041887	-0.005266	0.022936
21O	-0.217723	-0.221765	-0.237569	-0.004042	0.019846	-0.013383	0.041887	-0.007328	0.03598
22C	-0.029382	0.063389	-0.080058	0.092771	0.0506776	0.307164	0.167793	0.168193	0.091878
23C	0.330475	0.353250	0.265629	0.022775	0.064846	0.075408	0.214705	0.116865	0.117565

(*continued on next page*)

Table 11. (*Continued*)

Atom no.	Hirshfeld atomic Charges			Fukui functions		Local softnesses		Local electrophilicity indices	
	qN	qN $^{+}$ 1	qN $^{-}$ 1	f_k^+	f_k^-	Sk^+	Sk^-	ωκ+	ωk^-
24C	0.292636	0.326110	0.266726	0.033474	0.02591	0.110832	0.085788	0.060688	0.200938
25C	-0.102850	-0.030464	-0.180325	0.072386	0.077475	0.23967	0.256619	0.131235	0.140462
26C	0.154589	0.137111	0.133655	-0.017478	0.020934	-0.057869	0.069312	-0.031687	0.037953
27C	-0.005863	0.039626	-0.109637	0.045489	0.1041781	0.150614	0.344933	0.082471	0.188874
28C	0.021020	0.063678	-0.124660	0.042658	0.14568	0.14124	0.482346	0.077338	0.264117
29C	-0.079824	0.011960	-0.180409	0.091784	0.100585	0.303896	0.333036	0.166404	0.18236
30C	0.659322	0.640663	0.547728	-0.018659	0.111594	-0.061779	0.383877	-0.033828	0.202319
31O	-0.527831	-0.468488	-0.609557	0.059343	0.081726	0.196484	0.270594	0.107588	0.148169
32O	-0.521460	-0.505795	-0.520950	0.015665	-0.00051	0.051866	-0.001688	0.0284	-0.000924
33O	-0.498634	-0.456131	-0.478825	0.042503	-0.019809	0.140727	-0.065587	0.077057	-0.035913
36O	-0.253230	-0.203971	-0.314248	0.049259	0.061018	0.163096	0.20203	0.089306	0.110625
37O	-0.221030	-0.125157	-0.291115	0.095873	0.070085	0.317435	0.232051	0.173817	0.127064
38C	0.173484	0.243450	0.195045	0.069966	0.173484	0.231657	0.574405	0.126848	0.314526
39O	-0.204551	-0.206162	-0.233043	-0.001611	0.028492	-0.005334	0.94337	-0.00292	-0.002920

https://doi.org/10.1016/j.heliyon.2019.e01118

In Specioside (SS), the relative high value of local reactivity descriptors(f_k^+, S_k^+, ω_k^+) at C6, C18, C22, C24, C29 indicate that these sites to nucleophilic whereas the relative high value of local reactivity descriptors (f_k^-, S_k^-, ω_k^-) at C29, O30, O31, O33, C37 and O38 indicate this site to electrophilic attack (Table 10). In verminoside (VS), the relative high value of local reactivity descriptors(f_k^+, S_k^+, ω_k^+) at C6, C18, C22, C25, C29 indicate that these sites to nucleophilic whereas the relative high value of local reactivity descriptors (f_k^-, S_k^-, ω_k^-) at C30, O36, C37 and O38 indicate this site to electrophilic attack (Table 11).

4. Conclusion

In the present work, we have done comparative studies of two compounds i.e. Specioside (SS) and Verminoside (VS) which have been characterized by ^{1}H and ^{13}C NMR, UV−Visible and FT-IR analysis. Theoretical ^{1}H and ^{13}C chemical shift values (with respect to TMS) are reported and compared with experimental data which are in good agreement both for ^{1}H and ^{13}C NMR. The electronic properties are also calculated and compared with the experimental UV−Vis spectrum. It is concluded that the lowest singlet excited state of the molecule is mainly derived from the HOMO-LUMO (n- π^*) electron transition. Information of the charge density distribution and site of chemical activity of the molecule has been obtained by reactivity descriptors and MESP surface. NBO results reflected the charge transfer within the molecule. The calculated first hyperpolarizability of the Specioside (SS) compound is 55.8 $\times 10^{-30}$ esu and Verminoside (VS) is 3385.0111 for B3LYP level and these values are greater (429 times in case of specioside (SS) and approximately more than 25000 times in case of verminoside (VS)) for B3LYP than that of the standard NLO material urea (0.13×10^{-30} esu) that indicates the nonlinear optical applications. Furthermore, the thermodynamic parameters and electronic absorption properties of the compounds have been calculated. All the theoretical results show good agreement with experimental data. Fukui functions, local softness and electrophilicity indices for selected atomic sites have been calculated. Fukui function shows the nucleophilic and electrophilic attacking sites in the inhibitors. The local reactivity descriptors (f_k^-, S_k^-, ω_k^-) at C29, O30, O31, O33, C37 in specioside (SS) and O38, C30, O36, C37 and O38 in verminoside (VS) indicate that this site is more prone to electrophilic attack. Comparison of theoretical and experimental data exhibits good correlations confirming the reliability of the quantum chemical method to reveal the reactivity of the compounds.

Declarations

Author contribution statement

Monika Saini, Reetu Sangwan: Performed the experiments.

https://doi.org/10.1016/j.heliyon.2019.e01118

Mohammad Faheem Khan: Analyzed and interpreted the data.

Ashok Kumar, Ruchi Verma: Contributed reagents, materials, analysis tools or data.

Sudha Jain: Conceived and designed the experiments; Wrote the paper.

Funding statement

This work was supported by the University Grants Commission (UGC) and Council of Scientific and Industrial Research (CSIR), New Delhi. Mohd Khan was supported by Dr D. S. Kothari Postdoctoral Fellowship (letter no. F.4−2/2006 (BSR)/CH/13−14/0153) from UGC. Ashok Kumar was supported by UGC fellowship. Reetu Sangwan was supported by CSIR (FILE NO 09/107(0369)2014-EMR-I). Ruchi Verma was supported by UGC fellowship (RGNF) (F1-17.1/2014-15/RGNF-2014-SC-UTT-78865). The authors acknowledge the Department of Chemistry, University of Lucknow for computational and spectral analysis.

Competing interest statement

The authors declare no conflict of interest.

Additional information

No additional information is available for this paper.

References

[1] J. Hutchinson, J.M. Dalziel, H. Heine, in: second ed., in: N. Hepper (Ed.), Flora of Tropical West Africa, Vol. II, 1963, p. 385.

[2] J.M. Watt, M.G.B. Brandwijk, The Medicinal and Poisonous Plants of Southern and Eastern Africa, second ed., Pub. E. & S. Livingstone Ltd, 1962, p. 142.

[3] S.D. Lal, B.K. Yadav, Folk medicine of kurukshetra district (Haryana). India, Econ. Bot. 37 (3) (1983) 299−305.

[4] P.J. Houghton, The sausage tree (*Kigelia pinnata*): ethnobotany and recent scientific work, South Afr. J. Bot. 68 (1) (2002) 14−20.

[5] M.F. Khan, P. Dixit, N. Jaiswal, A.K. Tamrakar, A.K. Srivastava, R. Maurya, Chemical constituents of *Kigelia pinnata* twigs and their GLUT4 translocation modulatory effect in skeletal muscle cells, Fitoterapia 83 (1) (2012) 125−129.

[6] P.J. Houghton, D.N. Akuniyli, Iridoids from *Kigelia pinnata* bark, Fitoterapia 65 (1993) 473.

https://doi.org/10.1016/j.heliyon.2019.e01118

[7] S.F. El-Naggar, R.W. Doskotch, Specioside: a new iridoid glycoside from Catalpa speciosa, J. Nat. Prod. 43 (1980) 524−526.

[8] N. Bharti, S. Singh, F. Naqvi, A. Azam, Isolation and in vitro antiamoebic activity of iridoids isolated from *Kigelia pinnata*, Arkivoc 10 (10) (2006) 69−79.

[9] A. Jyotsna, A.K. Yadav, P. Aakanksha, P. Swapnil, M.M. Gupta, R. Pandey, Specioside ameliorates oxidative stress and promotes longevity in Caenorhabditis elegans, Comp. Biochem. Physiol. C 169 (2015) 25−34.

[10] P. Patrizia, A. Giuseppina, S. Marzocco, M. Meloni, R. Sanogo, R.P. Aquino, Anti-inflammatory activity of verminoside from kigelia a fricana and evaluation of cutaneous irritation in cell cultures and reconstituted human epidermis, J. Nat. Prod. 68 (2005) 1610−1614.

[11] O.A. Binutu, K.E. Adesogan, J.I. Okogun, Antibacterial and antifungal compounds from *Kigelia pinnata*, Planta Med. 62 (4) (1996) 352−353.

[12] J.A. Walsh, Problems in recognition and diagnosis of amebiasis: estimation of the global magnitude of morbidity and mortality, Rev. Infect. Dis. 8 (1986) 2228.

[13] WHO, Report of the expert consultation on amoebiasis, WHO Epidemiol. Record 4 (1997) 14.

[14] R. Mishra, B.D. Joshi, A. Srivastava, P. Tandon, S. Jain, Quantum chemical and experimental studies on the structure and vibrational spectra of an alkaloid−Corlumine, Spectrochim. Acta Mol. Biomol. Spectrosc. 118 (2014) 470−480.

[15] A.K. Srivastava, A.K. Pandey, S. Jain, N. Misra, FT-IR spectroscopy, intramolecular C− H··· O interactions, HOMO, LUMO, MESP analysis and biological activity of two natural products, triclisine and rufescine: DFT and QTAIM approaches, Spectrochim. Acta Mol. Biomol. Spectrosc. 136 (2015) 682−689.

[16] M.J. Frisch, G.W. Trucks, H.B. Schlegel, G.E. Scuseria, M.A. Robb, J.R. Cheeseman, J.A. Montgomery Jr., T. Vreven, K.N. Kudin, J.C. Burant, J.M. Millam, S.S. Iyengar, J. Tomasi, V. Barone, B. Mennucci, M. Cossi, G. Scalmani, N. Rega, G.A. Petersson, H. Nakatsuji, M. Hada, M. Ehara, K. Toyota, R. Fukuda, J. Hasegawa, M. Ishida, T. Nakajima, Y. Honda, O. Kitao, H. Nakai, M. Klene, X. Li, J.E. Knox, H.P. Hratchian, J.B. Cross, V. Bakken, C. Adamo, J. Jaramillo, R. Gomperts, R.E. Stratmann, O. Yazyev, A.J. Austin, R. Cammi, C. Pomelli, J.W. Ochterski, P.Y. Ayala, K. Voth, G.A. Morokuma, P. Salvador, J.J. Dannenberg, V.G. Zakrzewski,

 https://doi.org/10.1016/j.heliyon.2019.e01118

S. Dapprich, A.D. Daniels, M.C. Strain, O. Farkas, D.K. Malick, A.D. Rabuck, K. Raghavachari, J.B. Foresman, J.V. Ortiz, Q. Cui, A.G. Baboul, S. Clifford, J. Cioslowski, B.B. Stefanov, G. Liu, A. Liashenko, P. Piskorz, I. Komaromi, R.L. Martin, D.J. Fox, T. Keith, M.A. Al-Laham, C.Y. Peng, A. Nanayakkara, M. Challacombe, P.M.W. Gill, B. Johnson, W. Chen, Wong, M.W. Wong, C. Gonzalez, J.A. Pople, Gaussian 03, Revision C.02, Gaussian Inc., Wallingford, CT, 2004.

[17] M.J. Frisch, G.W. Trucks, H.B. Schlegel, G.E. Scuseria, M.A. Robb, J.R. Cheeseman, G. Scalmani, V. Barone, B. Mennucci, G.A. Petersson, H. Nakatsuji, M. Caricato, X. Li, H.P. Hratchian, A.F. Izmaylov, J. Bloino, G. Zheng, J.L. Sonnenberg, M. Hada, M. Ehara, K. Toyota, R. Fukuda, J. Hasegawa, M. Ishida, T. Nakajima, Y. Honda, O. Kit, H. Nakai, T. Vreven, J.A. Montgomery Jr., J.E. Peralta, F. Ogliaro, M. Bearpark, J.J. Heyd, E. Brothers, K.N. Kudin, V.N. Staroverov, R. Kobayashi, J. Normand, K. Raghavachari, A. Rendell, J.C. Burant, S.S. Iyengar, J. Tomasi, M. Cossi, N. Rega, J.M. Millam, M. Klene, J.E. Knox, J.B. Cross, V. Bakken, C. Adamo, J. Jaramillo, R. Gomperts, R.E. Stratmann, O. Yazyev, A.J. Austin, R. Cammi, C. Pomelli, J.W. Ochterski, R.L. Martin, K. Morokuma, V.G. Zakrzewski, G.A. Voth, P. Salvador, J.J. Dannenberg, S. Dapprich, A.D. Daniels, O. Farkas, J.B. Foresman, J.V. Ortiz, J. Cioslowski, D.J. Fox, Gaussian Inc., Wallingford, CT, 2009.

[18] Computer Program Gauss View 3.09, Gaussian Inc., P. A. Pittsburgh, 2003 [SD-008], Ver. 2.

[19] E. Frisch, H.P. Hratchian, R.D. Dennington II, T.A. Keith, J. Millam, A.B. Nielsen, A.J. Holder, J. Hiscocks, GaussView, Gaussian, Inc., 2009, Version 5.0.8.

[20] A.D. Becke, Density-functional thermochemistry. III. The role of exact exchange, J. Chem. Phys. 98 (1993) 5648−5652.

[21] T. Yanai, D. Tew, N. Handy, A new hybrid exchange−correlation functional using the Coulomb-attenuating method (CAM-B3LYP), Chem. Phys. Lett. 393 (2004) 51−57.

[22] C.T. Lee, W.T. Yang, R.G.B. Parr, Development of the Colle-Salvetti correlation-energy formula into a functional of the electron density, Phys. Rev. 37 (1988) 785−790.

[23] D.A. Petersson, M.A. Allaham, A complete basis set model chemistry. II. Open-shell systems and the total energies of the 1st-row atoms, J. Chem. Phys. 94 (1991) 6081−6090.

https://doi.org/10.1016/j.heliyon.2019.e01118

[24] G.A. Petersson, A. Bennett, T.G. Tensfeldt, M.A. Allaham, W.A.J. Mantzaris, A complete basis set model chemistry. I. The total energies of closed-shell atoms and hydrides of the first-row elements, J. Chem. Phys. 89 (1988) 2193–2218.

[25] K. Wolinski, J.F. Hinton, P. Pulay, Efficient implementation of the gauge-independent atomic orbital method for NMR chemical shift calculations, J. Am. Chem. Soc. 112 (1990) 8251–8260.

[26] E. Kraka, D. Cremer, Computer design of anticancer drugs. A new enediyne warhead, J. Am. Chem. Soc. 122 (2000) 8245–8264.

[27] R.G. Parr, W. Yang, Density Functional Theory of Atoms and Molecules, Oxford University Press, Oxford, 1989.

[28] R.G. Pearson, Chemical Hardness -Applications from Molecules to Solids, VCH, Wiley, Weinheim, 1997.

[29] P. Geerlings, F. Proft De, W. Langenaeker, Conceptual density functional theory, Chem. Rev. 103 (2003) 1793.

[30] P.K. Chattaraj, S. Giri, Stability, reactivity, and aromaticity of compounds of a multivalent superatom, J. Phys. Chem. 111 (43) (2007) 11116–11121.

[31] R.J. Mathar, Mutual conversion of three flavors of gaussian type orbitals, Int. J. Quant. Chem. 90 (1) (2002) 227–243.

[32] C.M. Compadre, J.F. Jauregui, P.J. Nathan, A.G. Enriquez, Isolation of 6-O-(p-Coumaroyl)-Catalpol from Tabebuia rosea1, Planta Med. 46 (1982) 42–44.

[33] L. Yin, L. Qiuxia, T. Shancai, D. Lisheng, G. Yiran, C. Fang, L. Tang, Bioactivity-guided isolation of antioxidant and anti-hepatocarcinoma constituents from Veronica ciliata, Chem. Cent. J. 10 (2016) 27.

[34] J.S. Al-Otaibi, R.I. Al-Wabli, Vibrational spectroscopic investigation (FT-IR and FT-Raman) using ab initio (HF) and DFT (B3LYP) calculations of 3-ethoxymethyl-1, 4-dihydroquinolin-4-one, Spectrochim. Acta Mol. Biomol. Spectrosc. 137 (2015) 7–15.

[35] A.Y. Musa, A.H. Kadhum, A.B. Mohamad, A.B. Rohoma, H. Mesmari, Electrochemical and quantum chemical calculations on 4, 4-dimethyloxazolidine-2-thione as inhibitor for mild steel corrosion in hydrochloric acid, J. Mol. Struct. 969 (2010) 233–237.

[36] G. Gece, S. Bilgic, Quantum chemical study of some cyclic nitrogen compounds as corrosion inhibitors of steel in NaCl media, Corros. Sci. 51 (2009) 1876–1878.

https://doi.org/10.1016/j.heliyon.2019.e01118

[37] A. Rahmani, M. Mirzaie, M. Rahmani, Structural properties, theory functional calculations (DFT), natural bond orbital acetamide and sulfonamide, Adv. Environ. Biol. 8 (6) (2014) 1703−1706.

[38] V. Vrajmasu, V.E. Munck, E.L. Bominaar, Theoretical analysis of the Jahn−teller distortions in tetrathiolato iron (II) complexes, Inorg. Chem. 43 (2004) 4862−4866.

[39] A. Frisch, A.B. Nelson, A.J. Holder, Gauss View, Inc., Pittsburgh, PA, USA, 2005.

[40] K.C. Chou, Biological functions of low-frequency vibrations (phonons). III. Helical structures and microenvironment, J. Biophysical. 45 (5) (1984) 881−889.

[41] X. Li, K.H. Hopmann, J. Hudecova, J. Isaksson, J. Novotna, W. Stensen, V. Andrushchenko, M. Urbanova, J.S. Svendsen, P. Bour, K. Ruud, Determination of absolute configuration and conformation of a cyclic dipeptide by NMR and chiral spectroscopic methods, J. Phys. Chem. 117 (2013) 1721−1736.

[42] S. Fatma, A. Bishnoi, A.K. Verma, Synthesis, spectral analysis (FT-IR, 1H NMR, 13C NMR and UV−visible) and quantum chemical studies on molecular geometry, NBO, NLO, chemical reactivity and thermodynamic properties of novel 2-amino-4-(4-(dimethylamino) phenyl)-5-oxo-6-phenyl-5, 6-dihydro-4H-pyrano [3, 2-c] quinoline-3-carbonitrile, J. Mol. Struct. 1095 (2015) 112−124.

[43] T. Gnanasambanadan, S. Gunasekaran, S. Seshadri, Vibrational spectroscopic investigation on propylthiouracil. Res. J. Chem. Environ. 17 (2013) 42−52.

[44] K. Druzbicki, E. Mikuli, M.D.O. Chrusciel, Experimental (FT-IR, FT-RS) and theoretical (DFT) studies of vibrational dynamics and molecular structure of 4-n-pentylphenyl-4′-n-octyloxythiobenzoate (8OS5), Vib. Spectrosc. 52 (2010) 54−62.

[45] D. Dolega, A.M. Mikuli, J. Chrusciel, Experimental (FT-IR, FT-RS) and theoretical (DFT) studies of vibrational dynamics and molecular structure of 4-n-pentylphenyl-4'-n-heptyloxythiobenzoate (7OS5), J. Mol. Struct. 933 (2009) 30−37.

[46] G. Varsanyi, Vibrational Spectra of Benzene Derivatives, Academic Press, New York, 1969.

[47] N.P.G. Roeges, A Guide to the Complete Interpretation of Infrared Spectra of Organic Structures, John Wiley and Sons Inc., New York, 1994.

https://doi.org/10.1016/j.heliyon.2019.e01118

[48] N.B. Colthup, L.H. Daly, S.E. Wiberly, Introduction to Infrared and Raman Spectroscopy, second ed., Academic Press, New York, 1975.

[49] N. Sundaraganesan, S. Ilakiamani, B.J. Dominic, Vibrational spectroscopy investigation using ab initio and density functional theory analysis on the structure of 3, 4-dimethylbenzaldehyde, Spectrochim. Acta, Part A 68 (2007) 680–687.

[50] D.F.V. Lewis, V.C. Ioannides, D.V. Parke, Interaction of a series of nitriles with the alcohol-inducible isoform of P450: computer analysis of structure-—activity relationships, Xenobiotica 24 (1994) 401–408.

[51] J. Wang, G. Jiande, J. Leszczynski, Phosphonylation mechanisms of sarin and acetylcholinesterase: a model DFT study, J. Phys. Chem. B 110 (2006) 7567–7573.

[52] W. Zhang, D.P. Curran, Synthetic applications of fluorous solid-phase extraction (F-SPE), Tetrahedron 62 (2006) 11837–11865.

[53] G. Lewandowski, E. Meissner, E. Milchert, Special applications of fluorinated organic compounds, J. Hazard 136 (3) (2006) 385–391.

[54] H. Endrédi, F. Billes, G. Keresztury, Revised assignment of the vibrational spectra of methylpyrazines based on scaled DFT force fields, J. Mol. Struct. THEOCHEM 677 (1–3) (2004) 211–225.

[55] S. Ghadah, Z. Alghamdi, Z. Ali, Z. Alzahrani, Bonding formation and orbitals nature of ZnO structure, J. Sci. Res. 13 (9) (2013) 1144–1149.

[56] J.B. Ott, J. Boerio-Goates, Calculations from Statistical Thermodynamics, Academic Press, 2000.

[57] D.F. Eaton, Nonlinear optical materials, Science 25 (1991) 281–287.

[58] D.A. Kleinman, Nonlinear dielectric polarization in optical media, Phys. Rev. 126 (1962) 1977–1979.

[59] D. Sajan, L. Josepha, N. Vijayan, M. Karabacak, Natural bond orbital analysis, electronic structure, non-linear properties and vibrational spectral analysis of L-histidinium bromide monohydrate: a density functional theory, Spectrochim. Acta Mol. Biomol. Spectrosc. 81 (2011) 85–98.

[60] R. Zhang, B. Dub, G. Sun, Y. Sun, Experimental and theoretical studies on o-, m-and p-chlorobenzylideneaminoantipyrines, Spectrochim. Acta Mol. Biomol. Spectrosc. 75 (2010) 1115–1124.

[61] J.L. Gazquez, Perspectives on the density functional theory of chemical reactivity, J. Mexican. Chem. Soc. 3 (2008) 52.

 https://doi.org/10.1016/j.heliyon.2019.e01118

[62] T. Koopmans, Über die Zuordnung von Wellenfunktionen und Eigenwerten zu den einzelnen Elektronen eines Atoms, Physica 1 (6) (1933) 104−113.

[63] R.G. Parr, R.G. Pearson, Absolute hardness: companion parameter to absolute electronegativity, J. Am. Chem. Soc. 105 (26) (1983) 7512−7516.

[64] R.G. Parr, L.V. Szentpály, S. Liu, Electrophilicity index, J. Am. Chem. Soc. 121 (9) (1999) 1922−1924.

[65] J. Padmanabhan, R. Parthasarathi, V. Subramaniaan, P.K. Chattaraj, Electrophilicity-based charge transfer descriptor, J. Phys. Chem. 111 (2007) 1358−1361.

[66] R.G. Pearson, Absolute electronegativity and hardness: applications to organic chemistry, J. Org. Chem. 54 (1989), 1430−14.

[67] R.G. Parr, W. Yang, Density functional approach to the frontier-electron theory of chemical reactivity, J. Am. Chem. Soc. 106 (1984) 404.

[68] K. Fukui, Role of frontier orbitals in chemical reactions, Science 218 (1987) 747.

[69] P.W. Ayers, M. Levy, Perspective on "Density functional approach to the frontier-electron theory of chemical reactivity", Thea. Chem. Acc. 103 (2000) 353.

[70] N. Islam, D.C. Ghosh, Evaluation of global hardness of atoms based on the commonality in the basic philosophy of the origin and the operational significance of the electronegativity and the hardness. Part I. The Gordy's scale of electronegativity and the GH, Eur. J. Chem. 1 (2) (2010) 83−89.

[71] E. Chamorro, P.K. Chattaraj, P. Fuentealba, Variation of the electrophilicity index along the reaction path, J. Phys. Chem. 107 (36) (2003) 7068−7072.

[72] A. Shukla, E. Khan, A. Srivastava, P. Tandon, K. Sinha, A computational study on molecular structure, multiple interactions, chemical reactivity and molecular docking studies on 6 [D (−) α-amino-phenyl-acetamido] penicillanic acid (ampicillin), Mol. Simulat. 42 (11) (2016) 863−873.

https://doi.org/10.1016/j.heliyon.2019.e01118